Laser-type cooling with unfiltered sunlight

Amanda Younes and Wesley C. Campbell
Department of Physics and Astronomy, University of California, Los Angeles, 90095 Los Angeles, California, USA

(Received 24 May 2023; accepted 1 February 2024; published 6 March 2024)

Cooling of systems to sub-Kelvin temperatures is usually done using either a cold bath of particles or spontaneous photon scattering from a laser field; in either case, cooling is driven by interaction with a well-ordered cold (i.e., low-entropy) system. However, there have recently been several schemes proposed for "cooling by heating," in which raising the temperature of some mode drives the cooling of the desired system faster. We discuss how to cool a trapped ion to its motional ground state using unfiltered sunlight at 5800 K to drive the cooling. We show how to treat the statistics of thermal light in a single-mode fiber for delivery to the ion and show experimentally how the blackbody spectrum is strongly modified by being embedded in quasi-one-dimension. Quantitative estimates for the achievable cooling rate with our measured fiber-coupled low-dimensional sunlight show promise for demonstrating this implementation of cooling by heating.

DOI: 10.1103/PhysRevE.109.034109

I. INTRODUCTION

Cooling is commonly accomplished by the coupling between a system of interest and a cold bath, with no further interactions. However, in some cases the coupling between the two is controlled by the occupation of some other mode that connects them. A good example of this is laser cooling, where the electromagnetic modes populated by laser photons allow the system of interest to repeatedly spontaneously emit into cold, nearly vacuum modes [1]. The cooling is thereby driven by the highly occupied modes of the laser, without which the cooling rate will fall to essentially zero.

However, since an ideal laser field is often approximated as in a coherent state [2], it is a displaced vacuum and has no entropy; the laser field can be thought of as being highly ordered and in that sense also extremely cold.[1] The lasers used for laser cooling tend to have very narrow linewidths (typically $\Delta\nu/\nu < 10^{-8}$ for laser cooling atoms and molecules), as that feature allows the absorption of laser photons to be velocity dependent. One can therefore ask the following: Is it necessary for laser cooling that the field that drives the cooling step (i.e., that couples the system to the cold bath) also be in a low-entropy state? If so, to what extent can we identify the highly ordered nature of *that* laser field, as opposed to the highly ordered nature of the nearly vacuum field, as being responsible for the cooling?

Here we propose how the phenomenon known as cooling by heating [3,4] can be used to illustrate the answer to these questions when applied with unfiltered thermal light. Cooling by heating refers to cases where the coupling between the system of interest and the cold bath can be increased by increasing the thermal occupation of a mode that couples the two and therefore the system can be cooled by heating that mode. This paradigm has been used to study some counterintuitive scenarios exhibiting cooling by heating [5–8] and open questions persist about the interplay between this phenomenon and quantum correlations [9] and dissipative generation of entangled states [3].

We begin by introducing an experimentally accessible scenario from atomic physics where a single trapped atomic ion is to be cooled to its quantum ground state via a repeated cycle. Unitary (and therefore reversible, entropy-conserving, and noncooling [10]) operations on the atom's state are driven by a laser, followed by a separate step where only sunlight is applied to cool the ion by coupling it to a cold vacuum mode. In this paper, we use *cooling* to refer to any process that can increase the peak phase-space density of *the system*, which we define to be the nucleus and electrons of a trapped atomic ion. Much like laser cooling, the near-vacuum modes of the electromagnetic field serve as the cold thermal bath in this scheme, and the field that couples the system to the bath is said to drive the cooling, as in "laser cooling" and "cooling by heating." We analyze the achievable temperature in the presence of multiple baths at different temperatures using a model of virtual qubits [11,12]. We then discuss the statistical physics of blackbody radiation confined in a single-mode optical fiber for delivery to the ion and observe how dimensionality affects the spectrum of a blackbody by analyzing fiber-coupled sunlight with a spectrometer. We conclude with an estimate of the achievable experimental cooling rate in this system.

II. COOLING AN ION BY APPLYING THERMAL LIGHT TO COUPLE IT TO THE VACUUM

The form of laser cooling that we will consider for this demonstration is known as resolved-sideband cooling [13,14] and has been implemented with lasers to cool ions [15], atoms [16], and micromechanical oscillators [17] to their quantum ground states of motion.

[1] A comet orbiting the Sun can still have a very cold temperature, even if its atoms' motional states have all been displaced to some large, average energy in our reference frame.

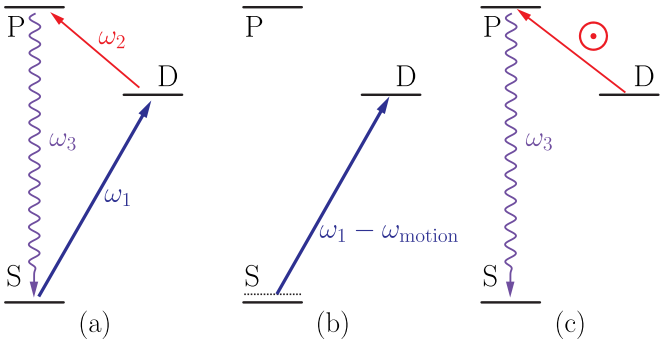

FIG. 1. Atomic level structure for sideband cooling. (a) Three-level atom with an $S \leftrightarrow D$ transition at ω_1, a $D \leftrightarrow P$ transition at ω_2, and an $S \leftrightarrow P$ transition at ω_3. (b) Step I of the cooling cycle, in which a red sideband of the $S \leftrightarrow D$ transition is driven by a laser at frequency $\omega_\ell = \omega_1 - \omega_{\text{motion}}$. (c) Step II of the cooling cycle, in which any population in D is returned to S via excitation to P from absorption of a photon at ω_2 followed by spontaneously emitting a photon at ω_3. We propose that the light at ω_2 can be provided by blackbody radiation from the Sun.

For a harmonically trapped atomic ion, the ion's motion in the trap is periodic at frequency ω_{motion} and this gives rise to the appearance of phase-modulated sidebands on the spectrum of applied laser light as observed in the rest frame of the ion. In the laboratory frame, this means that the ion's optical absorption spectrum consists of not only a carrier peak at the rest-frame resonant frequency of some optical transition (call it ω_1), but also sidebands at $\pm\omega_{\text{motion}}$ from the carrier (as well as at $\pm 2\omega_{\text{motion}}$ and so on). If the laser frequency ω_ℓ is set to be resonant with the feature at $\omega_\ell = \omega_1 - \omega_{\text{motion}}$ (the red sideband), the ion can absorb photons with energy $\hbar\omega_\ell$ but it will emit them with an average energy closer to $\hbar\omega_1$. Each cycle then removes approximately $\hbar\omega_{\text{motion}}$ of thermal energy on average, cooling the ion. Since the strength of the red sideband goes to zero as the ion's motion approaches the ground state, resolved-sideband cooling is capable of cooling the ion to its quantum ground state and then ceases to have any effect (in the absence of other sources of heating).

Since the spatial extent of the ion's harmonic motion ($x_0 = \sqrt{\hbar/2m\omega_{\text{motion}}}$, typically approximately equal to 5 nm) is much smaller than the wavelength of radiation at that frequency ($\lambda = 2\pi c/\omega_{\text{motion}}$, typically approximately equal to 1 km), it is a very poor antenna and the ion's motion is substantially impedance mismatched to electromagnetic radiation. In the absence of technical electric field noise, the motion of ions trapped inside room-temperature vacuum chambers remain out of equilibrium with the chamber for all relevant experimental timescales, and we will ignore any direct coupling between light and motion.

The scheme we consider for sideband cooling of a trapped ion is shown in Fig. 1 and consists of a repeated two-step cycle as follows. In step I [Fig. 1(b)] the ion is illuminated by a narrow-linewidth laser on the red sideband of the $S \to D$ transition. The intensity and illumination time are chosen to fully transfer population to the (long-lived) D state for ions with energy near their thermal average energy and then the laser is turned off. On average, this step can reduce the motional energy of the ion, but it also adds a much larger amount of total energy in the form of internal excitation. Entropy from the motional state has been partially transferred to the internal state of the ion in this unitary process.

Although the kinetic energy of the ion's center of mass has decreased in step I, this alone does not constitute cooling of the system, which includes the phase space of the electrons. To cool the ion, peak phase-space density must increase and entropy must therefore decrease. This strong cooling has been shown to be impossible with external potentials (whether static or time dependent) and instead requires a dissipative process [10]. Since step I is unitary and therefore reversible, the total entropy of the ion has not changed and the laser has not cooled the system.

In step II [Fig. 1(c)] the ion is illuminated with light capable of driving any population in the long-lived D state to a higher-lying P state (with resonant frequency ω_2) that can quickly decay to the ground S state by spontaneously emitting a photon (ω_3) into an approximately unoccupied mode (thermal states of optical-frequency modes at room temperature are close to the vacuum state). This step does not change the motional energy of the ion on average but does reduce the total energy since the ion returns to its internal ground state. However, unlike step I, this step is not reversible and the ion's entropy (and therefore temperature) has been reduced. The optical modes at frequency ω_3 contain information about the ion's motional state, which is to say that the spontaneously emitted photon carries away entropy. This is the cooling step in the process.

In a typical implementation of sideband cooling for applications in precision measurement or quantum information processing, step II is driven by a laser at ω_2. However, this light need not be coherent nor narrow in linewidth, as its only job is to couple the ion to the vacuum modes at ω_3. For this, we propose to use thermal light in the form of fiber-coupled blackbody radiation at $T_\odot \approx 5800$ K from the Sun. Even if this light has spectral density near ω_1 and ω_3, the driving of those transitions will not directly change the motional energy of the atom on average and this does not inhibit cooling to the ground state (see Appendix B).

A. Minimum achievable temperature

To estimate the minimum temperature that can be achieved with this scheme, we start with a steady-state version of the sequence shown in Figs. 1(b) and 1(c) to illustrate thermalization, for which we assume band-limited sunlight and utilize the concept of virtual qubits [11]. Following that, we analyze the time-dependent scheme with unfiltered sunlight and argue that it achieves the same limiting temperature insofar as both scenarios yield a predicted minimum temperature that is below what the limiting temperature will likely be in practice due to other heating effects (such as momentum diffusion from absorption and emission, or heating from electrical noise).

If we wish to apply principles of thermodynamic equilibrium to the trapped ion example in Fig. 1, we need to identify a bath that is brought into contact with the ion's motion to cool it. For this, we can simplify the time-dependent scheme into a steady-state scheme by assuming that both the narrowband laser light [Fig. 1(b)] and the sunlight ($T_2 = T_\odot$) that connects

levels D and P [Fig. 1(c)] are applied simultaneously and continuously and that the sunlight is band limited such that it does not connect either upper state to S. In this case, the $S \leftrightarrow P$ transition is driven by room-temperature ($T_3 = T_{\text{room}}$) blackbody radiation and we can model the effect of the laser on $S \leftrightarrow D$ as a thermal field with temperature $T_\ell \to \infty$.

The continuous interaction of these three subsystems, each with a unique temperature, with the ion's motion can be aggregated into an effective interaction of the motion with a single virtual qubit with splitting $\omega_{\text{V}} = \omega_{\text{motion}}$ held at a virtual temperature T_{V}, which is given by [11] (see also Appendix A)

$$T_{\text{V}} = \frac{\omega_{\text{V}}}{\frac{\omega_3}{T_3} - \frac{\omega_2}{T_2} - \frac{\omega_\ell}{T_\ell}} = \frac{\omega_{\text{motion}}}{\frac{\omega_3}{T_{\text{room}}} - \frac{\omega_2}{T_\odot}}. \tag{1}$$

In the limit that $\omega_3/T_{\text{room}} \gg \omega_2/T_\odot$, we conclude that the minimum achievable temperature is given by the virtual temperature

$$T_{\text{V}} \approx \frac{\omega_{\text{motion}}}{\omega_3} T_{\text{room}}. \tag{2}$$

A thermal state of motion at T_{V} has an average motional excitation of $\langle n_{\text{motion}} \rangle = [\exp(\beta_{\text{V}} \hbar \omega_{\text{motion}}) - 1]^{-1} \approx \exp(-\beta_{\text{V}} \hbar \omega_{\text{motion}})$, where $\beta_i^{-1} \equiv k_{\text{B}} T_i$. Since we expect $k_{\text{B}} T_{\text{room}} \ll \hbar \omega_3$, this corresponds to an ion in its ground state of motion ($T_{\text{V}} \approx 1$ μK and $\bar{n}_{\text{motion}} \approx 10^{-46}$). Even in the limit where T_{room} is replaced with $T_\odot$, the virtual temperature is cold enough to cool the ion to its ground state (see Appendix B). We stress here that there are many potential sources of heating in experiments that we have not attempted to capture with this analysis, which focuses only on the steady-state solution with thermal radiation fields (the blackbody limit). Our conclusion is that ground-state cooling is possible with this scheme, but we do not claim that it is necessarily practical to achieve cooling all the way to T_{V}.

For the time-dependent scheme of Figs. 1(b) and 1(c) with unfiltered sunlight, if the sunlight is left on long enough for the atom's internal states to equilibrate, the atomic energy distribution will be held at $T_\odot$. However, the periodic extinction of that light in step I, as well as in particular the case if we assume that the light is turned off at the end of the protocol and the ion's internal states are allowed to relax, indicates that the atomic internal temperature will equilibrate to T_{room}. As such, the effect of the laser is essentially to translate the motional thermal state to an energy scale set by ω_1 and allow that system to thermalize to T_{room}, followed by relaxation of that atomic excitation back to the energy scale of ω_{motion}. We therefore expect the motional temperature to be limited by these considerations to a scaled version of T_{room}, which is precisely the temperature in Eq. (2). This is also the blackbody limit for standard sideband cooling with laser light in a room-temperature vacuum chamber.

B. Excitation rate from fiber-coupled blackbody radiation

An atom illuminated by a focused beam of thermal light will not experience the same field as if it were inside a blackbody. Many modes will be in vacuum (or at least different thermal) states due to the anisotropy of the illumination, rather than in thermal states at the temperature of the blackbody. To calculate the excitation rate Γ of a two-level atom initially in its ground state (state manifolds $\{|e_i\rangle\}$ and $\{|g_i\rangle\}$ with degeneracies g_{e} and g_{g}, split by ω_{eg}) illuminated by focused incoherent light, we adopt an Einstein rate equation approach

$$\Gamma = B_{\text{ge}} \rho(\omega_{\text{eg}}) \tag{3}$$

$$= \frac{\pi^2 c^3}{\hbar \omega_{\text{eg}}^3} \frac{g_{\text{e}}}{g_{\text{g}}} A_{\text{eg}} \rho(\omega_{\text{eg}}), \tag{4}$$

where A_{eg} and B_{ge} are the Einstein A and B coefficients for the transition and $\rho(\omega_{\text{eg}})$ is the spectral energy density (energy per unit volume per unit angular frequency) at the ion's position at the transition frequency.

We consider that light from an ideal blackbody is coupled into an optical fiber with a single Gaussian transverse mode and this fiber's output is being imaged onto the atom with an imaging system having half-cone convergence angle ϑ. We will further suppose, to keep our analysis consistent with typical experimental hardware, that $\vartheta \ll 1$, which allows us to treat the optical system with the paraxial approximation. We will assume that the fiber-coupled thermal light is the only significant source of illumination to calculate the rate from that contribution alone.

In the typical, textbook treatment of blackbody radiation, the light inside a blackbody in equilibrium at temperature T is characterized by a constant isotropic spectral radiance $B(\omega)$ (power per unit solid angle, per unit area, per unit angular frequency) given by Planck's law of blackbody radiation

$$B_{\text{P}}(\omega) = \frac{\frac{\hbar \omega^3}{4\pi^3 c^2}}{\exp(\beta \hbar \omega) - 1}. \tag{5}$$

However, as we show in the next section, thermal light emerging from a single-mode fiber differs somewhat from a true blackbody and is more conveniently characterized instead by a power spectral density $S(\omega)$ (power per unit angular frequency of a single transverse spatial mode). If the imaging system is capable of focusing the fiber mode onto a (potentially frequency-dependent) effective mode area $A(\omega)$, the spectral energy density at the atom is given by

$$\rho(\omega) = \frac{S(\omega)}{c A(\omega)}, \tag{6}$$

which can be used with Eq. (4) to calculate the excitation rate.

Given an instantaneous excitation rate Γp_D from state D to state P (see Fig. 1) for an atom with probability p_D of being in state D, the rate at which this results in a spontaneous emission back to the ground state, which completes the step of removing one quantum of motion on average, will be

$$\dot{n}_{\text{motion}} = -\Gamma p_D \eta_{SP}, \tag{7}$$

where $\eta_{SP} \equiv A_{PS}/(A_{PS} + A_{PD})$ is the branching fraction of spontaneous emission from P to go back to S.

III. THERMAL LIGHT IN A SINGLE-MODE FIBER

The statistics of thermal light confined to quasi-one-dimension[2] (Q1D) has been discussed in various contexts, including Johnson-Nyquist noise [18,19], photonics [20,21], photovoltaic energy conversion [22], and extra spatial dimensions [23,24]. We do not therefore present a new theoretical result by deriving the power spectral density of blackbody radiation embedded in Q1D. Here we present an optics-oriented derivation to illustrate the origin of the spectrum we will use to compare to experimental observations and a brief discussion of how to reconcile the modified spectrum in the fiber with Planck's law.

We can consider a single-mode optical fiber (which is to say, some waveguide that only supports one transverse mode of the electromagnetic field at each frequency ω) of length L (later we will take $L \to \infty$) with periodic boundary conditions and light allowed to propagate in only one of the two possible directions. Assuming, for simplicity, that the effective index of refraction in the fiber is $n = 1$, the allowed frequencies will be $\omega_i = i \times 2\pi c/L$ and the density of states per polarization will therefore be $di/d\omega = L/2\pi c$.

The average rate of photons in mode i passing through a fixed reference plane in the fiber will be $\langle n_i \rangle c/L$, so the time-averaged power from mode i is $P_i = \hbar\omega_i \langle n_i \rangle c/L$, where $\langle n_i \rangle$ is the average number of photons in mode i. Summing over the two available polarizations, using $\langle n_i \rangle = [\exp(\beta\hbar\omega_i) - 1]^{-1}$ for the expected thermal population for a mode with splitting $\hbar\omega_i$ and temperature $T = 1/k_B\beta$, and taking the $L \to \infty$ limit, we have the total time-averaged power

$$P_{\text{total}} = \int_0^\infty d\omega \frac{\frac{\hbar\omega}{\pi}}{\exp(\beta\hbar\omega) - 1} = \frac{\pi}{6\hbar}\frac{1}{\beta^2}. \tag{8}$$

From the integrand, we identify the power spectral density for thermal light in a single-mode fiber,

$$S(\omega) = \frac{\frac{\hbar\omega}{\pi}}{\exp(\beta\hbar\omega) - 1}. \tag{9}$$

This expression was used by Nyquist to explain thermal noise in electrical circuits [18], but it is also the spectrum of power for thermal light coupled into a single-mode fiber.

The spectrum of $S(\omega)$ ($\propto \omega\langle n \rangle$) differs in shape from the spectral radiance given by Planck [$B_P(\omega) \propto \omega^3\langle n \rangle$] and the total power is proportional to T^2, as opposed to the more-familiar T^4 of the Stefan-Boltzmann law in three dimensions. Thermodynamics, however, requires that the two ends of the fiber, if brought into optical contact with two isolated blackbodies, will allow them to equilibrate through the fiber. How this is possible if the spectrum in the fiber has a different shape and peak position than the three-dimensional case can be resolved as follows. We consider two extremes for the transverse mode confinement in the fiber: (i) The divergence angle of light from the fiber end is independent of ω, which is approximately true for a total-internal-reflection interpretation of step-index fiber, and (ii) the mode area of the fiber is independent of ω, which is approximately true for a photonic crystal fiber. Cases that are intermediate between these two are likewise handled as follows.

For case (i), optical considerations dictate that the effective mode area $A(\omega)$ must be frequency dependent to maintain a frequency-independent solid angle Ω. For case (ii), $\Omega(\omega)$ must be frequency dependent to ensure that A is independent of frequency. For cases between these two extremes, the relationship between the area of a diffraction-limited mode and its solid angle is related to a well-known phase-space-volume theorem in antenna theory, namely, that their product must be equal to the square of the wavelength

$$A(\omega)\Omega(\omega) = \lambda^2 = \left(\frac{2\pi c}{\omega}\right)^2. \tag{10}$$

As pointed out by Dicke in the context of thermal noise in microwave systems [25], this connects the one-dimensional power spectral density to the radiance

$$B(\omega) = \frac{S(\omega)}{A(\omega)\Omega(\omega)}. \tag{11}$$

Since thermodynamics requires that this be equal to Eq. (5) in thermal equilibrium, this argument highlights that Eq. (10) is a basic consequence of Planck's law. The assignment of spectral radiance for single spatial modes is discussed in Appendix C.

Earlier we argued that the spectral energy density $\rho(\omega)$ at the center of the focus of an optical system imaging a single mode of thermal radiation onto a spot size $A(\omega)$ was given by Eq. (6). Since the spectral radiance of that light will have the same frequency dependence (spectrum) as Planck's law (5) but lower power, the thermal light can be called graybody radiation, and we can use the ratio of the energy spectral density to that inside an ideal blackbody to define an efficiency (or geometric grayness) factor for the thermal light delivery system,

$$G \equiv \frac{\rho(\omega)}{\rho_P(\omega)}, \tag{12}$$

where

$$\rho_P(\omega) = \frac{\omega^2}{\pi c^3} S(\omega) = \frac{\frac{\hbar\omega^3}{\pi^2 c^3}}{\exp(\beta\hbar\omega) - 1} \tag{13}$$

is the energy density inside an ideal blackbody.

Combining (6) with (10) and (13) allows us to write the geometric grayness as

$$G = \frac{\frac{\lambda^2}{4\pi}}{A(\omega)} = \frac{\Omega(\omega)}{4\pi}, \tag{14}$$

where $\Omega(\omega)$ is the solid angle of the mode of the imaging system. In the limit that the mode solid angle covers all of the available solid angle, we recover the ideal blackbody energy density and $G \to 1$.

IV. MEASURED POWER SPECTRUM OF FIBER-COUPLED SUNLIGHT

To observe the predicted spectrum and power spectral density of Eq. (9) and benchmark the optical power that

[2]We are deliberate in not to referring to this as one-dimensional light, which is a different topic entirely. Maxwell's equations treating the light in the fiber are fully three dimensional, and the embedding in quasi-one-dimension refers to the fact that there is only one mode available in each of the two transverse directions.

can be coupled onto a trapped ion, three fibers with distinct guiding regimes were employed: a single-mode step-index fiber, a single-mode photonic crystal fiber, and a step-index multimode fiber. The first two were discussed above and the multimode fiber was used to compare to the three-dimensional spectrum.

For each fiber, sunlight was coupled in using a roof-mounted, home-built Sun tracker and a commercial, aspheric fiber collimator lens as the collection optic. To keep sunlight maximally coupled, the collimator lens is much larger than the minimum diameter necessary to resolve the Sun from a point source (which would be a diameter of $D_{\min} \approx 100$ μm), allowing for steady coupling efficiency even with pointing instability. This system is able to maintain maximal coupling for many hours.

To estimate the effect of atmospheric absorption and scattering, as well as nonideal emission, we use a standard reference spectrum [26] for sunlight on the surface of the Earth for the case of a collecting lens oriented toward the Sun. We use the ratio of the ideal three-dimensional Planck spectrum to the standard spectrum to create the expected standard spectrum in Q1D. This spectrum is an average correction for the Sun at a specific elevation in specific atmospheric conditions and does not apply perfectly to our conditions at each measurement; the true correction varies somewhat depending on the elevation of the Sun, weather conditions, and pollution levels.

To measure the power spectrum of the fiber-coupled light, we measure the output with a fiber-coupled spectrometer (Thorlabs model No. CCS175). We correct the measured output with the response function provided by the manufacturer. For the single-mode fibers, we also correct for the wavelength dependence of light entering the spectrometer through a slit using the mode properties in the fiber specifications. This correction is done by treating the fiber mode as a Gaussian beam between the fiber tip and the slit and then cutting off parts of the beam that are blocked by the slit.

For the multimode fiber, Fig. 2 shows that we observe a frequency dependence similar to the standard three-dimensional Planck spectrum [Eq. (13)] since the fiber-coupled light can occupy many transverse modes. The vertical scale in this case is arbitrary, and we have roughly matched the height of the measured and predicted spectra to allow comparison of their shapes.

For the two single-mode fibers, the measured spectra are shown in black and red in Fig. 3. The shapes of these spectra are clearly modified from Planck's law in three dimensions (compare to Fig. 2). The predicted spectrum of Eq. (9) is shown in dark blue, along with a prediction that takes into account the empirical solar spectrum at the Earth's surface (shaded blue).

A drop-off in all three spectra can be seen at short wavelengths. This is in part caused by the effective range of the antireflective coating on the fiber collimator, which causes a bend around 580 nm.

To calibrate the vertical scale, a shortpass filter is inserted in front of the input collimator to remove light with wavelengths longer than $\lambda = 900$ nm, and the power delivered by the fiber is measured with a calibrated photodiode power meter. By matching this power to numerical integration of the measured spectrum, we obtain power spectral density.

By comparing this to Eq. (9), we obtain the delivery efficiency $\eta(\omega)$ as the ratio of our measured power spectral density to the ideal Q1D spectrum at $T_\odot$. In the visible and near-infrared regions, we find efficiencies of $\eta = 0.6$–0.9 under good seeing conditions with both types of single-mode fiber.

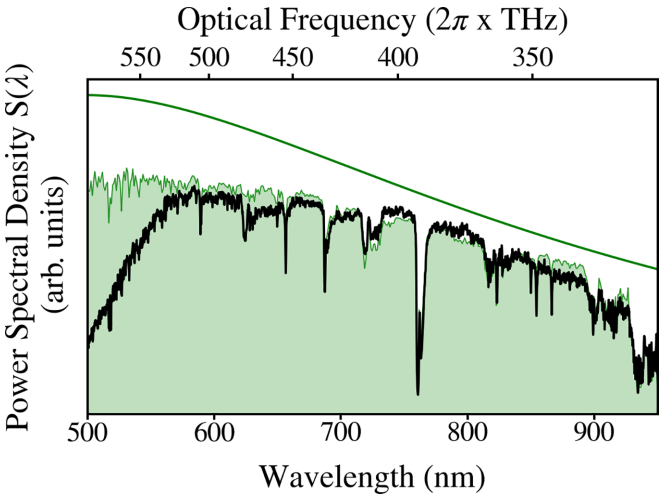

FIG. 2. Measured spectrum of sunlight coupled into a step-index, multimode optical fiber (black). The smooth green trace shows the theoretical frequency dependence of light emitted by an ideal three-dimensional blackbody, normalized to a peak height near the measured value to allow comparison. The shaded green-line trace shows the same theoretical spectrum with the atmospheric correction.

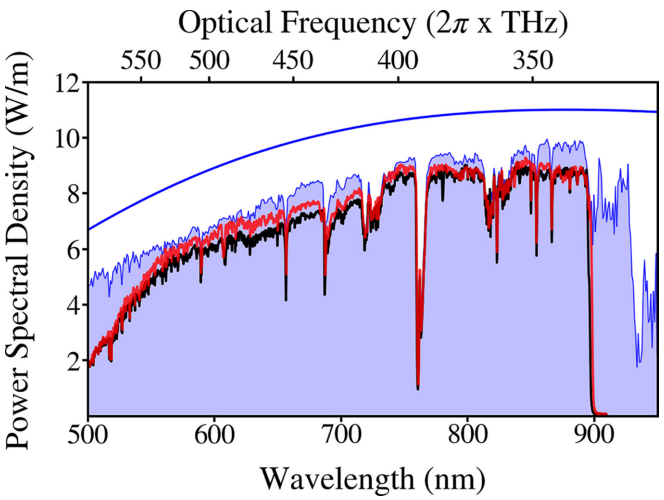

FIG. 3. Measured power spectral density of sunlight coupled into a single-mode step-index optical fiber (black) and a photonic crystal fiber (red), with wavelengths longer than 900 nm filtered out. The measured spectrum agrees with the theoretical curve for an ideal blackbody in Q1D [blue line, Eq. (9)] and the spectrum with atmospheric correction for the Q1D case (blue shaded region).

V. ESTIMATE OF COOLING RATE FROM MEASURED FIBER OUTPUT

We can now estimate the achievable cooling rate using fiber-coupled sunlight for our experimental parameters as follows. We consider a demonstration with Ba^+, for which the cooling light (ω_2 in Fig. 1) is near a wavelength of 614 nm.

Loss in 200 m of optical fiber from the roof to the laboratory is measured to be 35%–40% at this wavelength, giving an overall delivery efficiency of $\eta \approx 0.35$–0.60. For estimates of cooling rates, we use $\eta \approx 0.50$, which we have measured in the laboratory.

The imaging system is capable of focusing the fiber output to a spot size of $w_0 = 20$ μm, which corresponds to a geometric grayness of $G = 5 \times 10^{-5}$. The power spectral density in this mode can be related to Eq. (9) via

$$S_{\rm exp}(\omega_2) = \eta G S(\omega_2) \approx 2.5 \times 10^{-5} S(\omega_2). \tag{15}$$

Combining this power spectral density with the atomic parameters for Ba^+ yields an expected cooling rate of

$$\dot{n}_{\rm motion} = -8.2 \text{ phonons/s} \tag{16}$$

for initial motional states well above the ground state, which corresponds to approximately 0.4 mK/s for a mode frequency of $\omega_{\rm motion} = 2\pi \times 1$ MHz. Resolved sideband cooling is used starting near the Doppler limit, less than 1 mK for Ba^+. Heating rates that are comparable (smaller) in magnitude to (than) this cooling rate estimate ($\dot{n}_{\rm motion} < 10$ phonons/s) have been measured for ions in Paul traps [27–32], and lower rates ($\dot{n}_{\rm motion} < 1$ phonon/s) have been measured in Penning traps [33,34]. It therefore appears feasible that fiber-coupled sunlight may be capable of cooling a trapped ion to its ground state of motion.

While this approach with broadband thermal light is slower and less practical than the typical laboratory implementation of resolved sideband cooling with lasers, it provides a relatively simple and experimentally accessible example of cooling by heating. The possibility of achieving ground-state cooling using this method exposes the mechanism of cooling, which is not the low-entropy state of the laser mode as is commonly understood. Instead, the cooling is driven by the optical pumping (step II) or driving to a state that spontaneously emits a photon, carrying away entropy and cooling the ion.

ACKNOWLEDGMENTS

The authors acknowledge K. Barajas for discussions. This work was supported by the NSF under Grants No. PHY-2207985 and No. OMA-2016245.

APPENDIX A: DERIVATION OF VIRTUAL QUBIT TEMPERATURE

We consider the total Hilbert space of our system to be composed of a subspace for the motion of the ion, $\mathcal{H}_{\rm motion}$, with Hamiltonian $H_{\rm motion} = \hbar\omega_{\rm motion}(a^\dagger_{\rm motion}a_{\rm motion} + \frac{1}{2})$; the laser field $\mathcal{H}_\ell$ with Hamiltonian $H_\ell = \hbar\omega_\ell(a^\dagger_\ell a_\ell + \frac{1}{2})$; the field of the sunlight in the vicinity of ω_2, $\mathcal{H}_\odot$, with Hamiltonian $H_\odot = \hbar\omega_2(a^\dagger_\odot a_\odot + \frac{1}{2})$; and the atomic excitations $\mathcal{H}_{\rm atom}$ with Hamiltonian $H_{\rm atom} = \hbar\omega_3|P\rangle\langle P| + \hbar\omega_1|D\rangle\langle D|$. For a single cycle of the cooling scheme shown in Fig. 1, we need only consider a two-level subspace of the optical fields (which we will denote with primes, as in $\mathcal{H}'$) and we can consider them in the Fock basis as consisting of $|n\rangle$ and $|n-1\rangle$ photons for the state before and after an absorption event, respectively. For the atomic subspace, we can proceed by considering only the two-level system spanned by $|S\rangle$ and $|P\rangle$, and the Hamiltonian will be $H'_{\rm atom} = \hbar\frac{\omega_3}{2}\sigma_Z$, where we will refer to this two-level system with spin notation: $\sigma_Z \equiv |P\rangle\langle P| - |S\rangle\langle S|$. With these reduced versions, we can express the Hilbert space of interest as

$$\mathcal{H} = \mathcal{H}_{\rm motion} \otimes \mathcal{H}'_\ell \otimes \mathcal{H}'_\odot \otimes \mathcal{H}'_{\rm atom}. \tag{A1}$$

Following [12], we first consider that the cooling scheme is designed to ensure that the only way the atom can be excited to $|D\rangle$ is through the simultaneous annihilation of a phonon and a laser photon, the operator for which is $a_{\rm motion}a_\ell$. The cooling cycle then gives rise to an interaction Hamiltonian of the form

$$V \propto \left(a_{\rm motion}a_\ell a_\odot \sigma_+^{(\rm atom)} + a^\dagger_{\rm motion}a^\dagger_\ell a^\dagger_\odot \sigma_-^{(\rm atom)}\right), \tag{A2}$$

where $\sigma_+^{(\rm atom)} \equiv |P\rangle\langle S|$ is the atomic raising operator.

We can now identify the system that exchanges energy with the motion by defining the virtual qubit raising operator

$$\sigma_+^{(\rm V)} \equiv a_\ell a_\odot \sigma_+^{(\rm atom)} \tag{A3}$$

to cast (A2) in the form

$$V \propto \left(a_{\rm motion}\sigma_+^{(\rm V)} + a^\dagger_{\rm motion}\sigma_-^{(\rm V)}\right). \tag{A4}$$

The system now evolves in a smaller Hilbert space

$$\mathcal{H}' \equiv \mathcal{H}_{\rm motion} \otimes \mathcal{H}_{\rm V}, \tag{A5}$$

where the virtual qubit subspace is only two dimensional. The virtual qubit described by the raising operator (A3) has an energy splitting at frequency

$$\begin{aligned}\omega_{\rm V} &= -\omega_\ell - \omega_2 + \omega_3 \\ &= \omega_{\rm motion}.\end{aligned} \tag{A6}$$

To find the temperature of the virtual qubit, we apply the statistics of thermal equilibrium between the populations in the excited state $p_{\rm e}^{(i)}$ and the ground state $p_{\rm g}^{(i)}$ to each two-level subsystem [11],

$$\frac{p_{\rm e}^{(i)}}{p_{\rm g}^{(i)}} = \exp\left(-\frac{\hbar\omega_i}{k_{\rm B}T_i}\right), \tag{A7}$$

where $k_{\rm B}$ is the Boltzmann constant. We find

$$\begin{aligned}\exp\left(-\frac{\hbar\omega_{\rm V}}{k_{\rm B}T_{\rm V}}\right) &= \frac{p_{\rm e}^{(\rm V)}}{p_{\rm g}^{(\rm V)}} \\ &= \frac{p_{\rm g}^{(\odot)}p_{\rm g}^{(\ell)}p_{\rm e}^{(\rm atom)}}{p_{\rm e}^{(\odot)}p_{\rm e}^{(\ell)}p_{\rm g}^{(\rm atom)}} \\ &= \exp\left(\frac{\hbar\omega_2}{k_{\rm B}T_2} + \frac{\hbar\omega_\ell}{k_{\rm B}T_\ell} - \frac{\hbar\omega_3}{k_{\rm B}T_3}\right).\end{aligned} \tag{A8}$$

Solving (A8) for $T_{\rm V}$ gives

$$T_{\rm V} = \frac{\omega_{\rm V}}{\frac{\omega_3}{T_3} - \frac{\omega_2}{T_2} - \frac{\omega_\ell}{T_\ell}}. \tag{A9}$$

APPENDIX B: VIRTUAL TEMPERATURE IN CONTINUOUS SUNLIGHT

If we neglect the coupling to room-temperature blackbody radiation and assume, in the service of providing a conservative estimate of the achievable temperature, that both of the non-laser-addressed transitions can be driven by sunlight at $T_\odot$, we have

$$T_{\mathrm{V}} = \frac{\omega_{\mathrm{V}}}{\frac{\omega_3}{T_\odot} - \frac{\omega_2}{T_\odot} - \frac{\omega_\ell}{T_\ell}}. \tag{B1}$$

Again taking the limit as $T_\ell \to \infty$ yields

$$\begin{aligned} T_{\mathrm{V}} &= \frac{\omega_{\mathrm{motion}}}{\omega_3 - \omega_2} T_\odot \\ &= \frac{\omega_{\mathrm{motion}}}{\omega_1} T_\odot. \end{aligned} \tag{B2}$$

For alkaline-earth ions, $k_{\mathrm{B}} T_\odot < \hbar\omega_1$ and we see that even in this case, we expect most of the population to be in the motional ground state for a motional temperature given by (B2).

APPENDIX C: SPECTRAL RADIANCE OF SINGLE MODES

While Eq. (11) provides an explanation for how to connect the power spectral density of thermal light confined to Q1D to the spectral radiance of blackbody radiation in three dimensions, the spectral radiance of thermal light emerging from a single-mode fiber will be highly anisotropic. In order to predict the energy density at a particular position in space in the far field, the angular distribution is needed, and this depends upon the fiber's mode area.

For a single Gaussian mode of radiation ($1/e$ field radius w_0) there are multiple mode areas that could be assigned. For example, it is common to adopt the integrated intensity, or so-called top hat definition [35], $A_{\mathrm{TH}} \equiv P/I_{\max} = \int dA \exp(-2\rho^2/w_0^2) = \frac{\pi}{2} w_0^2$, where P is the power in the traveling-wave mode and $I_{\max}$ is the peak intensity at the center of the mode. This is attractive from a radiometry perspective since it is the area of a hole in an opaque screen that would pass the same power P from normally incident plane waves of intensity $I_{\max}$. Adopting this, with a straightforward application of paraxial Gaussian optics, we can write the angular distribution of the spectral radiance in the form

$$B(\omega, \theta) = \frac{S(\omega)}{A_{\mathrm{TH}}} \frac{2}{\pi} \left(\frac{\omega w_0}{2c}\right)^2 \exp\left[-2\sin^2(\theta) \Big/ \left(\frac{2c}{\omega w_0}\right)^2\right]. \tag{C1}$$

However, care must be used when interpreting this in the context of radiative thermal transport, as this would imply that the differential spectral radiance evaluated at the peak of the angular distribution, $\theta = 0$, exceeds the value of a Planckian blackbody by a factor of 4:

$$\begin{aligned} B_{\max}(\omega) d\Omega &= \frac{S(\omega)}{A_{\mathrm{TH}}} \frac{2}{\pi} \left(\frac{\omega w_0}{2c}\right)^2 d\Omega \\ &= S(\omega) \frac{4}{\lambda^2} d\Omega \\ &= 4 B_{\mathrm{P}}(\omega) d\Omega. \end{aligned} \tag{C2}$$

At first glance, this seems to violate thermodynamic principles. For example, one could imagine the use of a series of fibers that are all carrying thermal radiation from a source at temperature T to tile the full solid angle surrounding another body, thereby illuminating it with an approximately isotropic, average spectral radiance that is four times more powerful than that inside the source, which would allow it to equilibrate to a temperature exceeding the source.

However, while the mode area A_{TH} can be useful for describing the spatial distribution of power in a Gaussian mode, the mode itself technically spans an infinite transverse extent, and this infinite support precludes the tiling of space by adjacent orthogonal modes. If we instead sharply cut off the Gaussian spatial mode at finite radius R_{c} to allow adjacent modes to be spaced by $2R_{\mathrm{c}}$, the degradation in peak spectral radiance per mode caused by spreading of the angular distribution from diffraction at the cutoff must to be taken into account. For fixed total transmitted power spectral density per mode, the optimum cutoff radius is zero, asymptotically approaching a top-hat mode, for which the peak spectral density is a factor of 4 smaller than Eq. (C2). It may therefore be safest to use a well-defined finite support when defining the mode area for radiative thermal transport with Gaussian modes, as the mode itself requires a larger area than just its variance (or full width at half maximum) to retain the far-field behavior described by Gaussian optics.

The broader conclusion here is that care must be used when trying to use spectral radiance for single isolated modes, as the mode area (analogous to position) and the mode solid angle (analogous to momentum) of a single mode cannot be sharply defined simultaneously. A single-mode fiber emitting thermal radiation at temperature T is in many ways similar to a blackbody at T, but its emitted radiance is not isotropic and it does not follow the Lambert or Stefan-Boltzmann laws. Many of the results that may be familiar for three-dimensional Planckian blackbody radiation are not necessarily valid for an isolated spatial mode.

[1] W. D. Phillips, Nobel lecture: Laser cooling and trapping of neutral atoms, Rev. Mod. Phys. **70**, 721 (1998).

[2] R. J. Glauber, Coherent and incoherent states of the radiation field, Phys. Rev. **131**, 2766 (1963).

[3] A. Mari and J. Eisert, Cooling by heating: Very hot thermal light can significantly cool quantum systems, Phys. Rev. Lett. **108**, 120602 (2012).

[4] B. Cleuren, B. Rutten, and C. Van den Broeck, Cooling by heating: Refrigeration powered by photons, Phys. Rev. Lett. **108**, 120603 (2012).

[5] Y. Ma, Z.-q. Yin, P. Huang, W. L. Yang, and J. Du, Cooling a mechanical resonator to the quantum regime by heating it, Phys. Rev. A **94**, 053836 (2016).

[6] D. Z. Rossatto, A. R. de Almeida, T. Werlang, C. J. Villas-Boas, and N. G. de Almeida, Cooling by heating in the quantum optics domain, Phys. Rev. A **86**, 035802 (2012).

[7] M. T. Naseem and Ö. E. Müstecaplıoğlu, Ground-state cooling of mechanical resonators by quantum reservoir engineering, Commun. Phys. **4**, 95 (2021).

[8] Z. Yang, C. Zhao, R. Peng, J. Yang, and L. Zhou, Improving mechanical cooling by using magnetic thermal noise in a cavity-magnomechanical system, Opt. Lett. **48**, 375 (2023).

[9] C. J. Villas-Boas, W. B. Cardoso, A. T. Avelar, A. Xuereb, and N. G. de Almeida, Does "cooling by heating" protect quantum correlations? Quantum Inf. Process. **15**, 2021 (2016).

[10] W. Ketterle and D. E. Pritchard, Atom cooling by time-dependent potentials, Phys. Rev. A **46**, 4051 (1992).

[11] N. Brunner, N. Linden, S. Popescu, and P. Skrzypczyk, Virtual qubits, virtual temperatures, and the foundations of thermodynamics, Phys. Rev. E **85**, 051117 (2012).

[12] M. T. Mitchison, M. Huber, J. Prior, M. P. Woods, and M. B. Plenio, Realising a quantum absorption refrigerator with an atom-cavity system, Quantum Sci. Technol. **1**, 015001 (2016).

[13] D. Wineland and H. Dehmelt, Proposed $10^{-14}\ \Delta\nu < \nu$ laser fluorescence spectroscopy on Tl^{+} mono-ion oscillator III, Bull. Am. Phys. Soc. **20**, 637 (1975).

[14] H. G. Dehmelt, Entropy reduction by motional sideband excitation, Nature (London) **262**, 777 (1976).

[15] F. Diedrich, J. C. Bergquist, W. M. Itano, and D. J. Wineland, Laser cooling to the zero-point energy of motion, Phys. Rev. Lett. **62**, 403 (1989).

[16] S. E. Hamann, D. L. Haycock, G. Klose, P. H. Pax, I. H. Deutsch, and P. S. Jessen, Resolved-sideband Raman cooling to the ground state of an optical lattice, Phys. Rev. Lett. **80**, 4149 (1998).

[17] J. D. Teufel, T. Donner, D. Li, J. W. Harlow, M. S. Allman, K. Cicak, A. J. Sirois, J. D. Whittaker, K. W. Lehnert, and R. W. Simmonds, Sideband cooling of micromechanical motion to the quantum ground state, Nature (London) **475**, 359 (2011).

[18] H. Nyquist, Thermal agitation of electric charge in conductors, Phys. Rev. **32**, 110 (1928).

[19] B. M. Oliver, Thermal and quantum noise, Proc. IEEE **53**, 436 (1965).

[20] L. S. Fohrmann, A. Y. Petrov, S. Lang, D. Jalas, T. F. Krauss, and M. Eich, Single mode thermal emission, Opt. Express **23**, 27672 (2015).

[21] A. I. Fisenko and V. F. Lemberg, Black-body thermal radiative and thermodynamic functions of 1-dimensional self-assembly nanotubes, arXiv:1909.11181.

[22] A. De Vos, Thermodynamics of radiation energy conversion in one and in three physical dimensions, J. Phys. Chem. Solids **49**, 725 (1988).

[23] P. T. Landsberg and A. De Vos, The Stefan-Boltzmann constant in n-dimensional space, J. Phys. A: Math. Gen. **22**, 1073 (1989).

[24] H. Alnes, F. Ravndal, and I. K. Wehus, Black-body radiation with extra dimensions, J. Phys. A: Math. Theor. **40**, 14309 (2007).

[25] R. H. Dicke, The measurement of thermal radiation at microwave frequencies, Rev. Sci. Instrum. **17**, 268 (1946).

[26] ASTM G173-03, Standard tables for reference solar spectral irradiances: Direct normal and hemispherical on 37° tilted surface (ASTM International, West Conshohocken, 2020), available at https://www.astm.org/g0173-03r20.html.

[27] C. Roos, T. Zeiger, H. Rohde, H. C. Nägerl, J. Eschner, D. Leibfried, F. Schmidt-Kaler, and R. Blatt, Quantum state engineering on an optical transition and decoherence in a Paul trap, Phys. Rev. Lett. **83**, 4713 (1999).

[28] N. Daniilidis, S. Gerber, G. Bolloten, M. Ramm, A. Ransford, E. Ulin-Avila, I. Talukdar, and H. Häffner, Surface noise analysis using a single-ion sensor, Phys. Rev. B **89**, 245435 (2014).

[29] J. A. D. Randall, High-fidelity entanglement of trapped ions using long-wavelength radiation, Ph.D. thesis, Imperial College London, 2016.

[30] C. D. Bruzewicz, J. M. Sage, and J. Chiaverini, Measurement of ion motional heating rates over a range of trap frequencies and temperatures, Phys. Rev. A **91**, 041402(R) (2015).

[31] W. Li, S. Wolf, L. Klein, D. Budker, C. E. Düllmann, and F. Schmidt-Kaler, Robust polarization gradient cooling of trapped ions, New J. Phys. **24**, 043028 (2022).

[32] D. Kalincev, L. S. Dreissen, A. P. Kulosa, C.-H. Yeh, H. A. Fürst, and T. E. Mehlstäubler, Motional heating of spatially extended ion crystals, Quantum Sci. Technol. **6**, 034003 (2021).

[33] J. F. Goodwin, G. Stutter, R. C. Thompson, and D. M. Segal, Resolved-sideband laser cooling in a Penning trap, Phys. Rev. Lett. **116**, 143002 (2016).

[34] G. Stutter, P. Hrmo, V. Jarlaud, M. K. Joshi, J. F. Goodwin, and R. C. Thompson, Sideband cooling of small ion Coulomb crystals in a Penning trap, J. Mod. Opt. **65**, 549 (2018).

[35] A. E. Siegman, *Lasers* (University Science Books, Melville, 1986).